A proposal for a horizontal vector approach in 3D electrical resistivity tomography and its associated geometric factor

Churl Hyun Jo*

*Director of Research Division, Subsurface Information Technologies, Inc., D 609, 40 Imee-ro, Uiwang-si, Gyeonggi-do, Republic of Korea. Email: chjo@geeha.co.kr

ABSTRACT

Electrical resistivity tomography (ERT) is commonly implemented with collinear electrode arrays that measure only electric-field components along the survey line, neglecting horizontal variations in other directions. While this limitation is acceptable in 2D ERT, it can be significant in 3D settings with complex geometry and strong resistivity contrasts. To address this issue, we propose an approach to determining the total magnitude and direction of the horizontal electric field. Access to such vector information may provide a more representative characterization of the local surface response in complex 3D settings. Because this requires non-collinear measurements, a corresponding basis for consistent apparent-resistivity calculation is also needed. We therefore introduce a generalized geometric factor based on field-aligned virtual points (FAViPs), defined by the primary-field direction in a homogeneous medium, to provide a physically consistent basis for non-collinear horizontal measurements. Because these points are defined at an arbitrary measurement location, the resulting geometric factor can be applied to non-collinear electrode arrays in irregular survey geometries. By formalizing these basic physical principles, this work provides a theoretical basis for horizontal-vector measurements in 3D ERT. While practical implementation may be limited by current field logistics, this approach offers a theoretical option for 3D surveys involving complex environments where more flexible electrode configurations may be beneficial.

Key words: 3D Electrical resistivity tomography (3D ERT), total magnitude and direction of the horizontal electric field, non-collinear, Geometric factor, field-aligned virtual points (FAViPs)

INTRODUCTION

Electrical resistivity tomography (ERT) is commonly implemented along linear survey lines with collinear electrode arrays that measure only the inline component of the surface electric field. In geological settings with pronounced 3D structures and strong resistivity contrasts, however, restricting measurements to the inline component may overlook important information carried by the transverse component. In such environments, the horizontal electric field may deviate significantly from the survey-line direction, so that inline-only measurements represent only a partial projection of the local response. Direct measurement of the full horizontal electric-field vector—its magnitude and direction—may therefore offer a more informative representation of that response.

Attempts to access transverse or non-collinear responses are not new. According to Szalai and Szarka (2008a), early efforts to obtain both inline and transverse components appeared in former Soviet studies using non-collinear arrangements. Related concepts were later used in geothermal surveys employing bipole–dipole configurations (Risk et al., 1970; Keller et al., 1975), and null arrays for transverse measurements were introduced by Szalai et al. (2002). A more formal vector-type treatment was subsequently developed through the apparent-resistivity tensor, in which both horizontal components of the electric field are measured and interpreted in tensor or invariant form (Bibby, 1977; Varga et al., 2018). These studies demonstrated the feasibility and value of transverse or vector-like acquisition, but they did not provide a unified formulation of the full horizontal electric field applicable to arbitrary electrode orientations in 3D ERT.

Another related line of research concerns parameter-sensitivity studies of surface geoelectric arrays. Those studies showed that array responses are inherently multidimensional, with distinct *x*-, *y*-, and *z*-component contributions, non-negligible off-line sensitivity, and, in nonlinear or focused arrays, an enhanced role of the *y* component and so-called horizontal vectorial information (Szalai and Szarka, 2008b, 2008c). They also clarified the familiar trade-off between resolution and robustness among conventional arrays such as Schlumberger and Wenner-type configurations. However, these works were mainly concerned with array characterization and survey design. In contrast, the present study focuses on reformulating the measured physical quantity as a horizontal-vector quantity defined by both magnitude and orientation for conventional ERT practice. As quantitative interpretation ultimately relies on inversion, it is desirable to formulate this reformulated quantity in a way that can be incorporated consistently into existing 3D ERT workflows. Although 3D inversion frameworks have advanced considerably (Loke and Barker, 1996; Yi et al., 2003; Günther et al., 2006), no commonly used data formulation explicitly redefines

the conventional potential-difference datum as a local horizontal-vector quantity for routine ERT acquisition.

A fundamental challenge in implementing horizontal-vector measurements lies in the formulation of apparent resistivity. According to Parasnis (1975), apparent resistivity is effectively a standardized potential difference, which is obtained by normalizing the measured voltage using a geometric factor. However, conventional geometric factors are predominantly defined for collinear electrode layouts and implicitly assume that the potential-electrode pair is aligned with the local electric-field direction produced by the current electrodes. Although certain special configurations may satisfy this condition by coincidence, measurements taken in arbitrary horizontal directions cannot, in general, be standardized consistently using conventional geometric factors. Previous attempts to generalize geometric factors (Bibby and Risk, 1973; Keller et al., 1975) or to formulate vector-based approaches such as the apparent-resistivity tensor (Bibby, 1977) still relied on configuration-specific settings, multiple-source measurements, or tensor/invariant formulations rather than a generalized geometric factor for a single horizontal-vector measurement. Other studies explored topographic effects (e.g., Bièvre et al., 2018) or expanded azimuthal coverage using L- and CORNER-type arrays (Tejero-Andrade et al., 2015), but these also remained geometry-specific. Within this framework, the study does not aim to replace the conventional geometric factor with an entirely new definition, but rather to define a corresponding geometric factor for non-collinear horizontal measurements on the basis of the physical principle that had been implicit in conventional geometric-factor derivations: potential-difference standardization should follow the electric-field direction, which in turn follows the potential gradient. In this way, horizontal electric field measurements can be extended beyond conventional inline-only measurements, and a corresponding basis for apparent-resistivity calculation can be defined consistently.

The work is therefore intended as a conceptual and theoretical formulation, rather than as a comprehensive evaluation of field-scale implementation or full 3D inversion performance. Its central contribution lies in making explicit a physical principle that has long remained implicit in conventional configurations: potential-difference standardization should be aligned with the direction of the local primary field defined for a homogeneous medium by the given current-electrode configuration. The present study generalizes this principle for arbitrary electrode geometries. Quantitative performance evaluation through full 3D inversion and field-scale validation remain essential next steps, but both presuppose the theoretical foundation established here and are therefore left for future research.

HORIZONTAL ELECTRIC FIELD VECTOR MEASUREMENT

Redefinition of potential-difference measurement

Let us reconsider the basis of potential-difference measurements in ERT. Traditionally in the conventional collinear configuration, the potential difference has been regarded as the potential measured between two electrodes placed along the line connecting the current electrodes. Based on this viewpoint, the midpoint between these two potential electrodes is defined as the *potential-difference measurement center* (hereafter the PoDiM center). The measurement is then considered as the potential difference between two points symmetrically positioned at a distance of $\Delta x/2$ from this center, where Δx is the electrode spacing, while maintaining the same inline orientation.

This scalar, inline representation can be generalized into a horizontal vector framework, which is essential for measuring the full complexity of 3D electric fields. For the common case in which the measurement plane is the ground surface, the electric field has two horizontal components, E_x and E_y. Thus its magnitude and direction must be determined from two orthogonal potential-difference pairs that measure the local field. A practical approach is to place two mutually perpendicular electrode pairs on a circle of radius $\Delta x/2$, with the PoDiM center (Figure 1). This configuration allows both the magnitude and direction of the horizontal electric field to be determined, while maintaining a consistent electrode spacing.

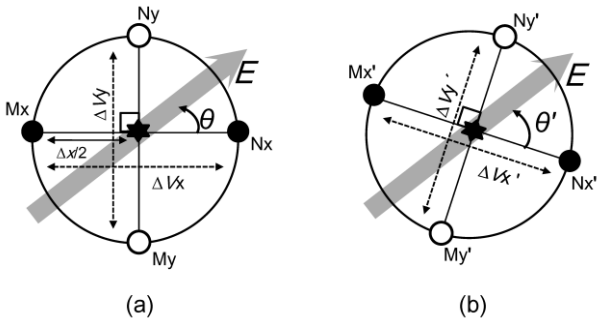

Figure 1. (a) Concept of the potential-difference measurement circle (radius $\Delta x/2$) centered on the potential-difference measurement center (asterisk). Two mutually perpendicular potential-electrode pairs (M_x–N_x and M_y–N_y) measure the potential differences ΔV_x and ΔV_y, demonstrating that both the magnitude and direction of the horizontal electric field (gray arrow **E**) can be obtained. (b) Rotated electrode pairs on the same circle illustrate that any orthogonal configuration provides equivalent measurements.

From this consideration, we define a revised form of potential-difference measurement in electrical prospecting: the measurement is taken between an electrode pair located at antipodal

points on a circle centered at the PoDiM center, with radius equal to half the electrode spacing, $r = \Delta x/2$. We refer to this construction as the *potential-difference measurement circle* (hereafter the PoDiM circle). In this configuration, the potential differences ΔV_x and ΔV_y are measured across two orthogonal electrode pairs (M_x–N_x and M_y–N_y), respectively, conceptually enabling the determination of both the magnitude and the direction of the horizontal electric field (Figure 1). This definition provides the basis for consistently treating potential differences in both collinear and non-collinear configurations.

To further illustrate the physical quantities obtainable from this scheme, consider Figure 1, from which the following relations can be derived for ERT measurements:

$$V_{total} = \sqrt{(\Delta V_x)^2 + \left(\Delta V_y\right)^2} = \sqrt{(\Delta V_x')^2 + \left(\Delta V_y'\right)^2} \quad (1)$$

$$\theta = \mathrm{atan2}\left(E_y,\ E_x\right) = \mathrm{atan2}\left(-dV_y, -dV_x\right) \quad (2)$$

where ΔV_x and ΔV_y denote the corresponding potential differences measured over equal electrode spacings (Δx=Δy), and $\Delta V'$ terms denote the corresponding potential differences measured at the same PoDiM circle but under a rotated electrode orientation. $\Delta V_{\mathrm{total}}$ represents the total magnitude of the potential difference at the PoDiM center, and θ is the azimuth of the horizontal electric field, with E_x and E_y being its components in the x and y directions, respectively. These quantities constitute the most fundamental observables in the proposed horizontal vector approach for 3D ERT.

Electric-field behavior in complex structure and limitations of conventional arrays

The most widely applied configurations in ERT are the Wenner–Schlumberger, dipole–dipole, pole–dipole, and pole–pole arrays, including their variants. Except for the pole–pole array, these configurations are fundamentally collinear. In 2D ERT, collinear arrays are almost exclusively adopted, so the measured potential difference represents only the inline component of the electric field, consistent with the 2D assumption of most inversion algorithms. In the widely used collinear arrays, the survey line is aligned with the straight line connecting the two current electrodes, and the electric field is assumed to be directed solely along this line. Accordingly, the measured potential difference, ΔV, has conventionally been regarded as the representative potential difference, although it actually represents only the component along the survey line:

$$\Delta V = \Delta V_x \tag{3}$$

where ΔV denotes potential difference in the conventional sense, whereas ΔV_x represents the actual potential difference measured along the survey line (the x-axis). In practice, ΔV has long been interpreted as the complete potential difference between two electrodes, although it in fact reflects only the component projected onto the survey line—an assumption that holds only when the electric field is nearly aligned with that line.

However, in real 3D settings, this assumption does not generally hold. Subsurface resistivity is inherently 3D, and under complex geometry and strong resistivity contrasts, the surface electric field may deviate significantly from the survey-line direction. Restricting measurements to the inline component therefore cannot fully represent the surface electric field and ultimately limits the accuracy of resistivity estimates.

To illustrate the directional complexity of the surface electric field, we constructed a 3D synthetic model consisting of a conductive arrow-shaped body embedded in a resistive host medium. The model geometry, survey layout, and electrode configuration are shown in Figure 2, and the modeling parameters are summarized in Table 1. Unless otherwise stated, the results presented below correspond to a base resistivity contrast of 1000:1, representing a high-contrast near-surface environment; a higher contrast of 10000:1 is additionally considered to illustrate pronounced directional distortion.

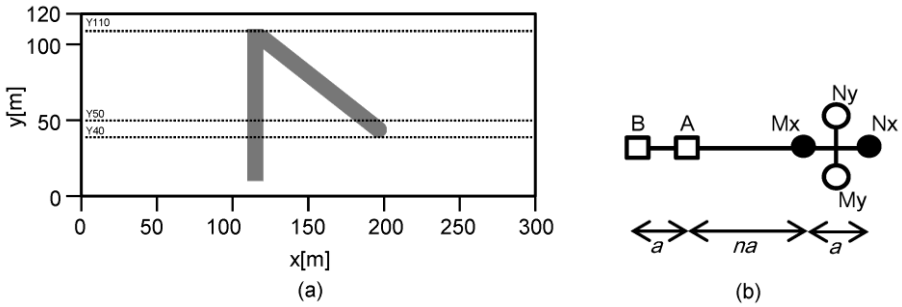

Figure 2. Schematic model and survey configuration used for the 3D ERT simulations. (a) Plan view of the arrow-shaped conductive anomaly embedded in a layered host medium. Selected profiles (Y110, Y50, and Y40) used in Figure 9 are indicated. (b) Dipole–dipole array schematic: current electrodes A (source) and B (sink); inline potential pair M_x–N_x; transverse potential pair M_y–N_y.

Table 1. Numerical modeling parameters used in the synthetic example.

Parameter	Value / Description
Numerical method	3D finite-element method (FEM)
Solver	PARDISO direct sparse solver
Grid size (Core)	N_x=121, N_y=49, N_z=41
Padding Layers	4 layers added on all side boundaries and 5 layers at the bottom; none for the surface
Grid spacing	2.5 m (uniform); padding spacing increases outward by factors of 2, 4, 8, and 16 (max. 40m)
Host medium	1 kΩ·m (base case); 10 kΩ·m (higher contrast)
Topsoil	100 Ω·m, 10 m thick, flat layer
Conductive	Arrow-shaped, 1 Ω·m, extending from 10 to 50 m depth, 10 m thick

Forward simulations were carried out using a dipole–dipole array with a fixed electrode spacing of 10 m along multiple parallel survey lines spanning x = 0–300 m. Although simulations were performed for a range of survey lines and electrode separations (n = 1–10), the results presented here focus on a representative case along the y = 40 m line, with the current electrodes located at x = 120–130 m. The resulting horizontal electric-field vectors are shown in Figure 3, demonstrating that even along nominally collinear survey lines, the field direction deviates markedly from the line orientation. In the higher contrast (Figure 3b), the field direction may locally reverse, resulting in a negative inline component ($\Delta V_x < 0$) due to the influence of the conductive anomaly.

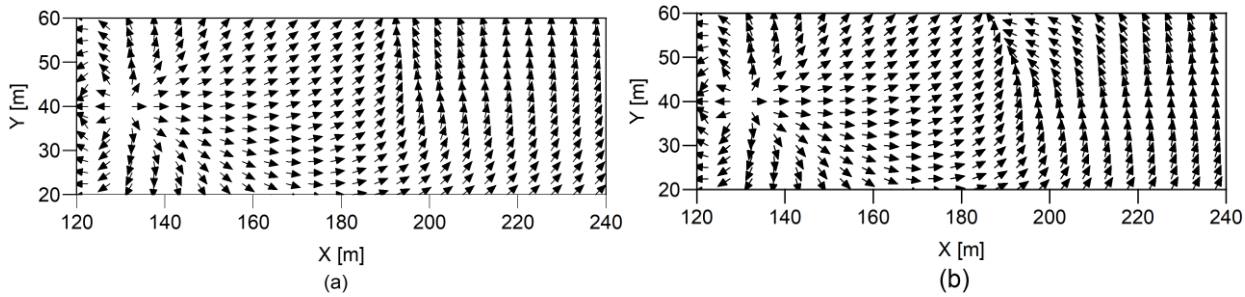

Figure 3. Horizontal electric-field vectors for the dipole–dipole configuration along the y = 40 m survey line, with current electrodes located at x = 120–130 m. Potential-electrode positions corresponding to n = 1–10 extend from x = 140 m to 240 m. Vectors are plotted at a depth of z = 1.25 m, corresponding to the midpoint of the first cell below the surface. (a) Base resistivity contrast of 1000:1. (b) Higher contrast case of 10000:1.

To quantify this effect, two diagnostic parameters were derived for the representative survey line (y = 40 m) shown in Figure 3 and are presented in Figure 4. Results are shown for both the primary

(1000:1) and higher (10000:1) contrast cases: (i) θ_E, the azimuth of the horizontal electric field (Figure 4a), and (ii) the ratio of the inline to total potential difference, $|\Delta V_x|/\Delta V_{\text{total}}$ (Figure 4b).

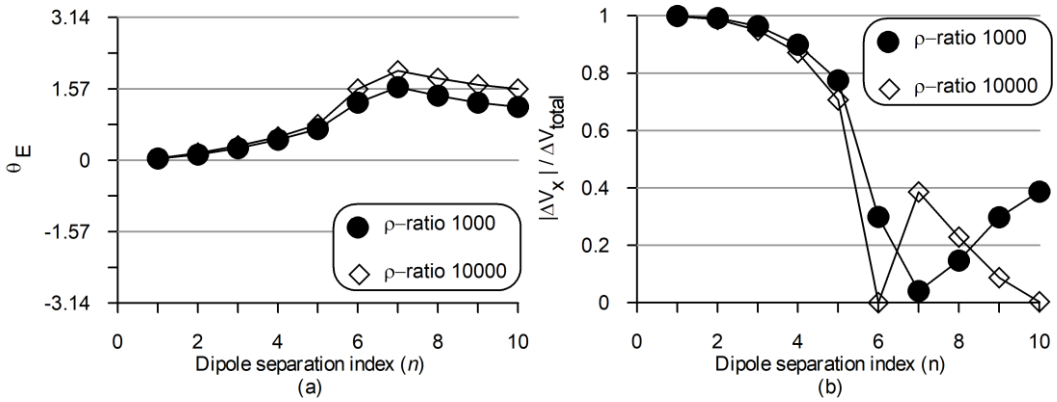

Figure 4. Quantitative characteristics of the horizontal electric field for the representative case shown in Figure 3: (a) azimuth of E (θ_E = atan2(E_y, E_x)); (b) ratio of the inline to total potential difference ($|\Delta V_x| / \Delta V_{\text{total}}$).

In the azimuth map (Figure 4a), the field direction exhibits pronounced deviations—approaching 90° and even locally reversing—when crossing the boundary of the conductive anomaly in the high-contrast case (10000:1). At these same locations, the inline potential difference becomes negative, producing negative apparent-resistivity values that conventional inline-only formulations cannot accommodate. The ratio map (Figure 4b) shows that the inline component may account for less than 50% of the total potential difference. Such a reduction in the inline component does not merely indicate directional distortion; it also exaggerates the apparent expression of conductive anomalies in conventional collinear surveys. Because the inline potential difference decreases when the true electric field rotates away from the survey line, the anomaly appears more conductive than it actually is. Thus, although the inferred position or geometry of an anomaly may be inaccurate, the anomaly itself often becomes more conspicuous—explaining why conventional 2D collinear ERT has remained effective for qualitative reconnaissance despite measuring only the inline component of the field.

Field observations also support this conclusion. For example, in highly resistive crystalline terrains of Korea, ERT surveys have occasionally yielded negative potential differences along survey lines (Jung *et al*., 2009). Such observations are commonly attributed to strong conductivity contrasts and complex subsurface geometry, further emphasizing the importance of accounting for electric-field direction when interpreting ERT data.

Horizontal vector measurements in 3D ERT interpretation and inversion

The horizontal vector measurement concept introduced above provides a framework for recording both the magnitude and the orientation of the surface electric field. We propose extending the conventional inline potential-difference measurement into two complementary parameters: (i) the apparent resistivity—often expressed in logarithmic form—derived from the total potential difference as defined in equation (1), and (ii) the azimuth of the horizontal electric-field vector as defined in equation (2). These parameters can be incorporated as complementary inversion inputs, possibly enhancing sensitivity to resistivity contrasts and improving the reconstruction of complex subsurface structures that cannot be adequately resolved by measurements of the conventional inline component.

A subsequent question then arises: how should the geometric factor be defined for non-collinear electrode configurations used in horizontal vector measurements? This leads to the next step of our formulation, in which a more generalized geometric factor is developed to handle non-collinear, irregular, and arbitrarily oriented electrode configurations, providing a consistent basis for apparent resistivity calculation in 3D ERT.

FIELD-ALIGNED GEOMETRIC FACTOR FORMULATION

Electric field in a homogeneous medium

In a homogeneous, isotropic half-space, the potential V_0 at a point P due to a current electrode pair (A, B; with A as source and B as sink) is expressed as

$$V_0(P) = \frac{\rho_0 I}{2\pi}\left(\frac{1}{R_{AP}} - \frac{1}{R_{BP}}\right), \tag{4}$$

where I is the injected current, ρ_0 is the medium resistivity, and R_{QS} denotes the distance between points $\boldsymbol{Q}$ and $\boldsymbol{S}$. The electric field $\mathbf{E}_0$ is the negative gradient of the potential V_0 ;

$$\mathbf{E_0}(P) = -\nabla V_0(P). \tag{5}$$

In this formulation, the resistivity and the current act only as multiplicative scaling factors. Thus, in a homogeneous isotropic medium, the direction of the electric field is determined solely by the geometry of the current electrodes, independent of resistivity or current. This invariant directional field pattern is hereafter referred to as *the primary field*. The primary field $\mathbf{E}_0$ defined here is a theoretical reference field for a homogeneous half-space. It serves as an invariant geometric baseline determined solely by the current-electrode configuration and is entirely independent of any

actual subsurface resistivity distribution. In contrast, the electric field measured in heterogeneous media may differ in both magnitude and direction from the primary field $\mathbf{E}_0$.

In collinear configurations, the primary-field direction coincides with the line connecting the current electrodes and therefore with the orientation of conventional collinear potential-electrode pairs. At off-line locations, however, the primary-field direction generally departs from the survey-line orientation. Figure 5 illustrates the primary field, and Figure 6 introduces the virtual points located along this direction.

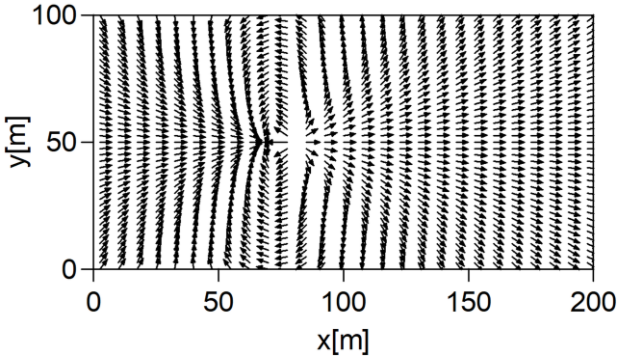

Figure 5. Vector plot of electric field generated by a current dipole in a homogeneous half-space. The source and sink poles are located at (80, 50) and (70, 50), respectively.

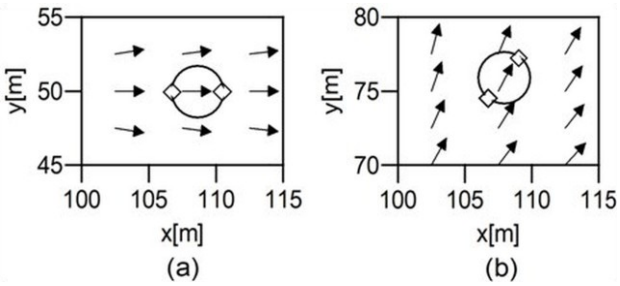

Figure 6. Enlarged view of the electric-field directions from Figure 5. Blank diamonds indicate two virtual points placed along the local field direction. (a) Along the line connecting the current electrodes, the field direction coincides with this line. (b) At an off-line point, the field direction deviates from the line connecting the current electrodes.

Definition of field-aligned virtual points (FAViPs)

Building on the above conceptual framework, we now formalize the determination of the local primary-field orientation at an arbitrary PoDiM center P with coordinates $(x_P,\ y_P)$. The positive

and negative current electrodes are located at $A\ (x_A,\ y_A)$ and $B\ (x_B,\ y_B)$, respectively, and r denotes half the potential-electrode spacing—equivalently, the radius of the PoDiM circle.

Before defining the field direction, the sign convention for potential difference should be clarified. In mathematical-physical notation, the potential variation along a positive direction may be expressed as $dV_x = V(x+dx) - V(x)$. Applied to the orthogonal PoDiM pair, this would give $dV_x = V(N_x) - V(M_x)$ and $dV_y = V(N_y) - V(M_y)$. In conventional resistivity surveying, however, the measured potential difference is defined in the opposite electrode order as $\Delta V = V(M) - V(N)$, so that the measured response is conventionally taken as positive in standard array configurations. The present study adopts this conventional survey definition consistently, because it preserves the usual positive sign of the geometric factor and apparent resistivity in a homogeneous half-space.

Two mutually orthogonal potential-electrode pairs, which we denote as the theoretical primary-field pairs M_{0x}–N_{0x} and M_{0y}–N_{0y} (Note: In practical field applications, these theoretical positions can be used as the physical electrode locations M_x and M_y for convenience.), are placed on the PoDiM circle to measure the local primary-field components:

$$M_{0x} = (x_P - r, y_P),\ N_{0x} = (x_P + r, y_P)\ ,$$

$$M_{0y} = (x_P, y_P - r),\ N_{0y} = (x_P, y_P + r)\ . \tag{6}$$

The potential differences across the two orthogonal pairs in a homogeneous medium are then given by

$$\Delta V_{0Px} = \frac{I\rho_0}{2\pi}\left\{\left(\frac{1}{R_{AM_{0x}}} - \frac{1}{R_{BM_{0x}}}\right) - \left(\frac{1}{R_{AN_{0x}}} - \frac{1}{R_{BN_{0x}}}\right)\right\},$$

$$\Delta V_{0Py} = \frac{I\rho_0}{2\pi}\left\{\left(\frac{1}{R_{AM_{0y}}} - \frac{1}{R_{BM_{0y}}}\right) - \left(\frac{1}{R_{AN_{0y}}} - \frac{1}{R_{BN_{0y}}}\right)\right\}. \tag{7}$$

Using a finite-difference approximation over an interval of $2r$, the primary local horizontal electric-field components are approximated as

$$E_{0x} \approx \frac{\Delta V_{0Px}}{2r}, \quad E_{0y} \approx \frac{\Delta V_{0Py}}{2r}. \tag{8}$$

Thus, the primary-field orientation θ_0 at P is obtained as

$$\theta_0 = atan2\left(E_{0y}, E_{0x}\right) \approx atan2\left(\Delta V_{0Py}, \Delta V_{0Px}\right). \tag{9}$$

This formal derivation explicitly connects the primary field—which is invariant regardless of subsurface anomalies—with the electrode geometry. The two antipodal points on the PoDiM circle that lie in the direction of this local primary-field orientation θ_0 are given by,

$$P_{v1} = (x_{\mathrm{P}} - r\cos\theta_0, y_{\mathrm{P}} - r\sin\theta_0),\ P_{v2} = (x_{\mathrm{P}} + r\cos\theta_0,\ y_{\mathrm{P}} + r\sin\theta_0\ ). \tag{10}$$

We designate P_{v1} and P_{v2} as the *field-aligned virtual points* (FAViPs) associated with point *P*. These may also be referred to simply as *principal points* in the context of formulating the generalized geometric factor. This definition does not introduce a new physical concept, but rather makes explicit a basic physical principle that has long remained implicit in conventional collinear configurations. Certain non-collinear arrays, such as equatorial arrays, also satisfy this alignment condition under their specific geometric circumstances.

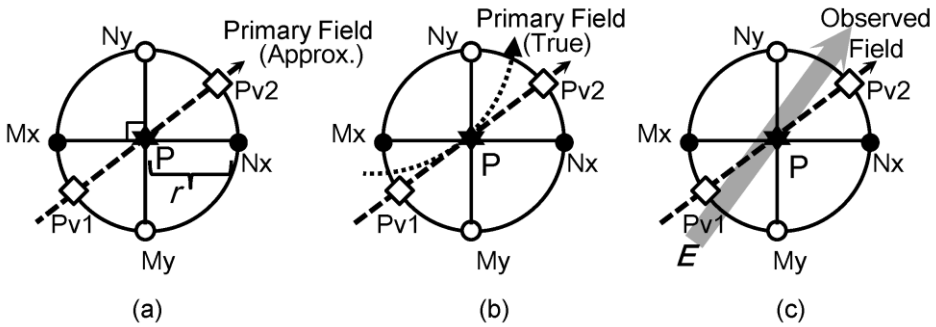

Figure 7. (a) Construction of the field-aligned virtual points (FAViPs) on the PoDiM circle. (b) Schematic illustration of primary-field curvature relative to the straight-line approximation. (c) The horizontal electric field measured in heterogeneous media using perpendicular potential-electrode pairs.

Figure 7a illustrates the construction of the FAViPs. At the PoDiM center, the local primary-field direction θ_0—which is determined solely by the electrode geometry in a homogeneous medium—is extended as a straight line to intersect the PoDiM circle, and the two intersection points define P_{v1} and P_{v2}. Crucially, since these FAViPs are anchored to the virtual primary field rather than the actual observed field, they remain spatially invariant regardless of the complexity or position of subsurface anomalies. Consequently, the determination of these points and the resulting geometric factor requires no a priori knowledge of the actual subsurface structure.

Due to the inherent curvature of the electric field lines—except along the dipole axis, the straight line connecting the current electrodes—the actual intersection of these curved primary-field lines with the PoDiM circle deviates slightly from the straight-line approximation used to define P_{v1} and P_{v2}. This theoretical distinction between the curved field line and the straight-line approximation is shown schematically in Figure 7b. In contrast, Figure 7c presents the actual observed horizontal electric field in heterogeneous media, where the field orientation deviates more significantly from the virtual primary reference θ_0 because of subsurface resistivity contrasts.

With these definitions, the geometric factor evaluated at *P* using the two FAVIPs is

$$G = \left\{\left(\frac{1}{R_{AP_{v1}}} - \frac{1}{R_{BP_{v1}}}\right) - \left(\frac{1}{R_{AP_{v2}}} - \frac{1}{R_{BP_{v2}}}\right)\right\}^{-1}. \quad (11)$$

More generally, this framework remains well-posed for arbitrary, non-collinear configurations because the FAViPs are constructed directly from the local primary-field direction at an arbitrary PoDiM center *P*, thereby providing a consistent reference for potential-difference normalization independent of electrode alignment. This generalized definition reduces to the conventional collinear geometric factor when P_{v1} and P_{v2} lie on the survey line connecting *A* and *B*.

VERIFICATION OF THE GENERALIZED GEOMETRIC FACTOR

To examine the validity of the generalized geometric factor derived from the FAViP framework, we evaluated whether a homogeneous half-space resistivity can be correctly recovered using analytically computed electric-field values. In the classical concept introduced by Parasnis (1975), apparent resistivity is interpreted as a standardized potential difference, normalized by a geometric factor that depends solely on array configuration. By analogy, our verification assesses whether the generalized geometric factor—defined within the FAViP concept—returns the true half-space resistivity when applied to analytically derived electric-field pairs.

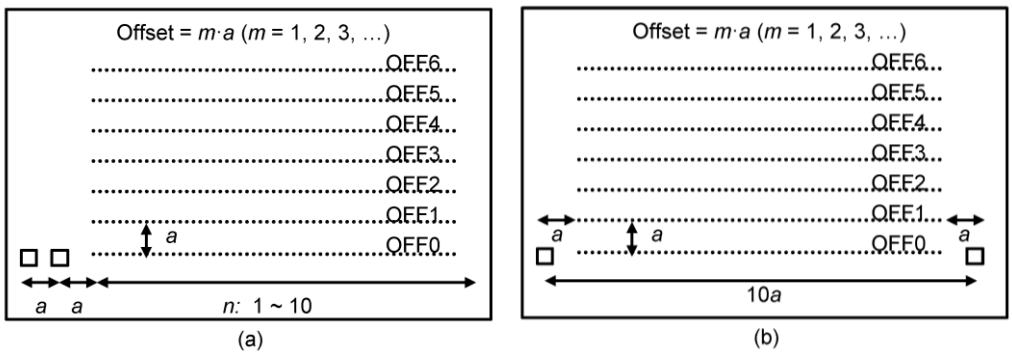

Figure 8. (a) Extended dipole–dipole (exterior-potential) configuration. (b) Extended Schlumberger (interior-potential) configuration. Current electrodes (squares) and the corresponding ranges of potential-electrode positions (dotted segments) used for evaluating the generalized geometric factor.

For clarity and generality, all electrode spacings are expressed in terms of an arbitrary unit length *a*. The PoDiM circle diameter is therefore *a*, and all offsets from the survey line are expressed as multiples *ma* (*m*=0, 1, … , 10). In Figure 8, the offset labels (OFF0, OFF1, OFF2, …) implicitly represent offsets of 0*a*, 1*a*, 2*a*, … expressed in units of the electrode spacing *a*. This notation is consistent with that used in Tables 2 and 3, where offsets are explicitly written as OFF*ma*. Using this notation, and following the layouts in Figure 8, two representative electrode configurations

were considered: an extended dipole–dipole array, corresponding to the exterior-potential pair configuration of Szalai and Szarka (2008), and an extended Schlumberger array, representing the interior-potential pair configuration.

The apparent resistivity at the PoDiM center P was calculated from the total potential difference magnitude ΔV_{total} and the FAVIP-based geometric factor G via

$$\rho_a = \frac{2\pi}{I}\,\Delta V_{total} \cdot G \quad . \tag{12}$$

The horizontal potential-difference components obtained from equations (1) and (7), together with the geometric factor in (11), were used to compute analytical apparent-resistivity values for both array types.

The normalized apparent resistivities, ρ_a/ρ_0, are presented in Table 2 and Table 3. Table 2 corresponds to extended dipole–dipole arrays (dipole length a, dipole separations n=1−10). Table 3 corresponds to extended Schlumberger arrays with PoDiM centers located at 1.5a–8.5a. In both configurations, the normalized apparent resistivities remain within approximately 1 % of the true resistivity over most offsets. Deviations increase to around 10 % only near the current electrode. In practical ERT surveys, variations of this magnitude may be typically regarded as negligible. These localized errors arise from the intrinsic curvature of the electric field, which persists even in a homogeneous medium (Figure 7b). The FAViP-based geometric factor assumes a straight-line approximation to the field direction within the PoDiM circle. Thus, near the source electrodes—where field curvature is strongest—small residual discrepancies are expected. Away from the sources, the PoDiM circle becomes effectively small relative to the radius of curvature, and the approximation becomes highly accurate.

Table 2. Normalized apparent resistivity ρ_a/ρ_0 for extended dipole-dipole arrays

n	OFF0	OFF1	OFF2	OFF3	OFF4	OFF5	OFF6	OFF7	OFF8	OFF9	OFF10
1	1.00	0.87	0.96	1.01	1.02	1.01	1.01	1.01	1.00	1.00	1.00
2	1.00	0.96	0.95	0.98	1.00	1.01	1.01	1.01	1.01	1.00	1.00
3	1.00	0.99	0.97	0.98	0.99	1.00	1.00	1.00	1.00	1.00	1.00
4	1.00	0.99	0.98	0.98	0.99	0.99	1.00	1.00	1.00	1.00	1.00
5	1.00	1.00	0.99	0.99	0.99	0.99	0.99	1.00	1.00	1.00	1.00
6	1.00	1.00	0.99	0.99	0.99	0.99	0.99	1.00	1.00	1.00	1.00
7	1.00	1.00	1.00	0.99	0.99	0.99	0.99	1.00	1.00	1.00	1.00
8	1.00	1.00	1.00	1.00	0.99	0.99	0.99	1.00	1.00	1.00	1.00
9	1.00	1.00	1.00	1.00	1.00	1.00	1.00	1.00	1.00	1.00	1.00
10	1.00	1.00	1.00	1.00	1.00	1.00	1.00	1.00	1.00	1.00	1.00

Table 3. Normalized apparent resistivity ρ_a/ρ_0 for extended Schlumberger arrays

PoDiM Center	OFF0	OFF1	OFF2	OFF3	OFF4	OFF5	OFF6	OFF7	OFF8	OFF9	OFF10
1.5a	1.00	0.92	0.96	0.98	0.99	1.00	1.00	1.00	1.00	1.00	1.00
2.5a	1.00	0.98	0.98	0.98	0.99	0.99	1.00	1.00	1.00	1.00	1.00
3.5a	1.00	1.00	0.99	0.99	1.00	1.00	1.00	1.00	1.00	1.00	1.00
4.5a	1.00	1.00	1.00	1.00	1.00	1.00	1.00	1.00	1.00	1.00	1.00
5.5a	1.00	1.00	1.00	1.00	1.00	1.00	1.00	1.00	1.00	1.00	1.00
6.5a	1.00	1.00	0.99	0.99	1.00	1.00	1.00	1.00	1.00	1.00	1.00
7.5a	1.00	0.98	0.98	0.98	0.99	1.00	1.00	1.00	1.00	1.00	1.00
8.5a	1.00	0.92	0.96	0.98	0.99	1.00	1.00	1.00	1.00	1.00	1.00

DISCUSSION

Formation of FAViPs

The formation of field-aligned virtual points (FAViPs) can be summarized as follows: (i) A local coordinate system is defined for the ERT project. (ii) Within this system, a PoDiM (potential-difference measurement) center and its corresponding PoDiM circle are specified. (iii) Two potential-electrode pairs are placed on the PoDiM circle along the local x- and y-axes as defined in equation (6). These pairs may serve as either virtual points for theoretical evaluation or actual electrodes used for field measurement. (iv) Using the coordinates of the current electrodes, the orientation of the virtual primary field (θ_0)—which serves as a purely geometric reference—is determined. Based on this fixed orientation, the FAViPs are defined on the PoDiM circle, and the corresponding generalized geometric factor is calculated.

This procedure provides a unified geometric framework that links the electrode configuration, the local primary field orientation, and the geometric factor. By grounding the normalization of potential differences in the fundamental relationship $\mathbf{E} = -\nabla\Phi$, this approach bridges theoretical vector physics with practical field implementation without requiring any a priori knowledge of the subsurface.

Illustrative 2D inversion example using horizontal vector measurements

To illustrate the practical implications of incorporating horizontal vector measurements, a simple 2D inversion test was performed using synthetic data along three representative profiles (Y110, Y50,

and Y40) from the model shown in Figure 2a**.** Data were generated using a dipole–dipole array with a dipole length of 10 m and a separation index ranging from n = 1 to 10. A resistivity contrast of 1000:1 was considered, and for each profile both the conventional inline-only data (ΔV_x) and the full horizontal potential-difference (ΔV_{total}) were inverted using DIPRO, a 2D inversion software based on Yi et al. (2003). The inversion results are shown in Figure 9.

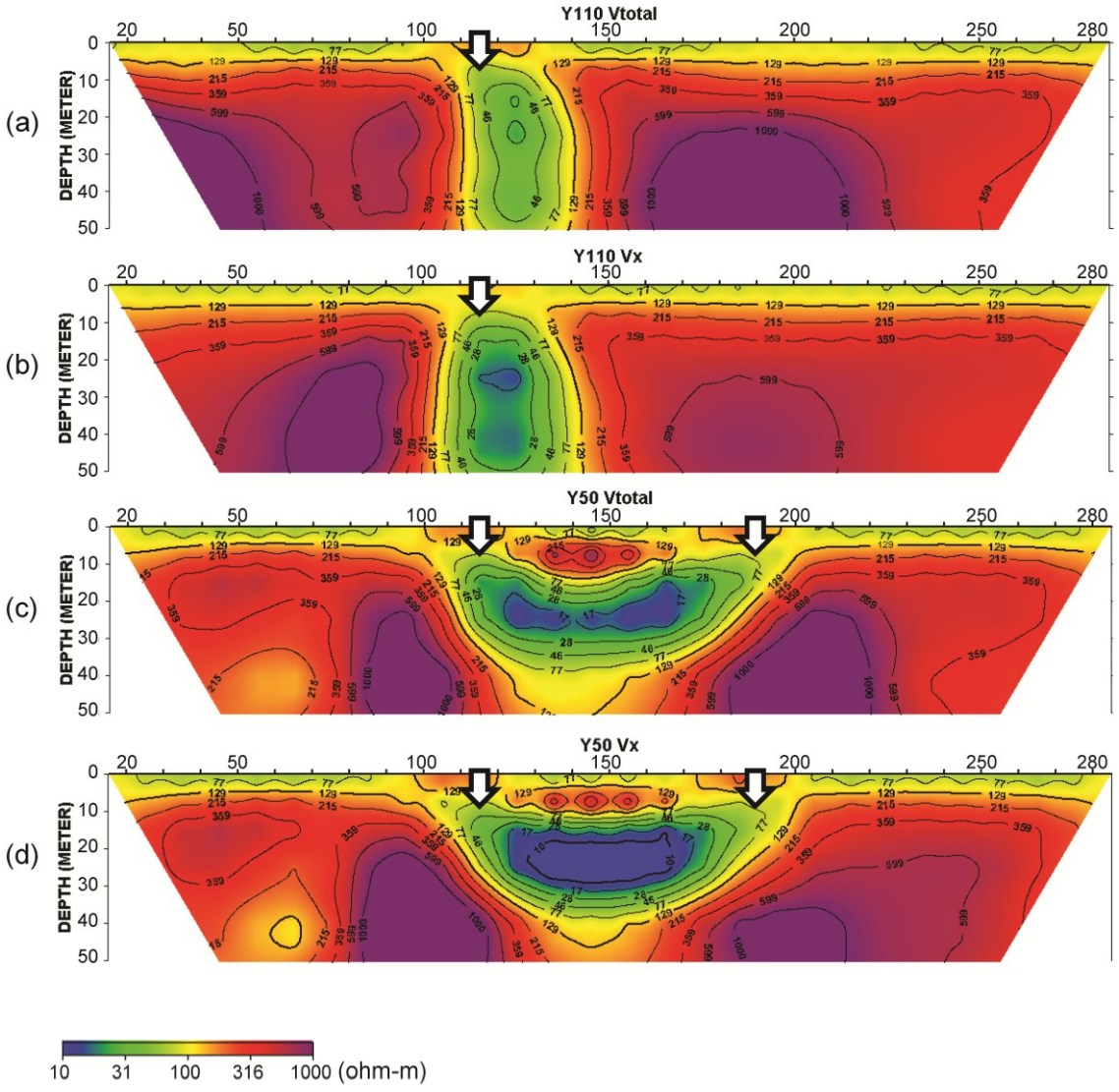

Figure 9. Illustrative 2D inversion results for three representative profiles (Y110, Y50, and Y40) from the model shown in Figure 2a, comparing inversions based on full horizontal potential-difference data (ΔV_{total}) and conventional inline-only data (ΔV_x), with a resistivity contrast of 1000:1. (a)-(b) Y110, ΔV_{total} and ΔV_x; (c)-(d) Y50, ΔV_{total} and ΔV_x

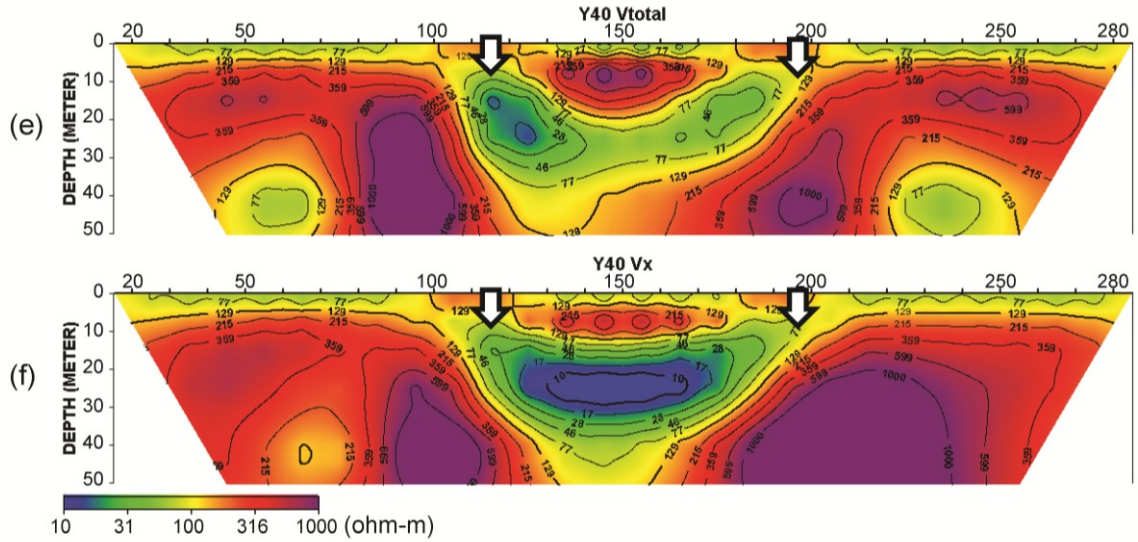

Figure 9(continued). (e)-(f) Y40, ΔV_{total} and ΔVx. Arrows indicate the position of the conductive anomaly.

The selected profiles were chosen to represent progressively stronger effects of field-direction deviation relative to the survey line. In the Y110 profile, the overall inversion patterns from ΔV_{total} and ΔV_x are similar and no clear advantage of either approach is observed. In the Y50 profile, the difference becomes more noticeable. In the Y40 profile, which crosses the boundary of the conductive anomaly where the directional deviation is strongest, the ΔV_{total} inversion yields more distinct anomaly boundaries and reduced lateral smearing compared to the ΔV_x inversion. This improvement does not result from any modification of the inversion algorithm itself, but is likely attributable to the use of a more representative potential-difference input.

Although this example is not intended as a full 3D inversion study, it provides supporting evidence that horizontal vector measurements can improve anomaly delineation even within conventional 2D inversion frameworks. This improvement appears even though directional information is not explicitly incorporated into the 2D inversion itself. If future 3D inversion schemes directly utilize horizontal electric-field vectors, further improvement in resolution may be possible.

Implications for 3D inversion

The proposed framework is a rigorous generalization of the geometric factor, formalizing the physical alignment that was previously only implicit in collinear arrays. Measuring the horizontal

electric-field vector incorporates transverse field information, which may increase sensitivity to lateral resistivity variations. This additional directional information may improve the conditioning of 3D inversion, particularly where strong lateral contrasts are present. The potential relevance of such measurements also extends to applications such as anisotropic inversion, in which field orientation plays an important role.

The proposed horizontal vector measurements can be incorporated into existing 3D inversion frameworks by utilizing their core algorithmic structures. While the underlying forward modeling kernels remain essentially the same, the integration process involves extending the data representation and sensitivity mappings to account for the magnitude and azimuth of the horizontal electric-field vector. Rather than a fundamental redesign of the inversion algorithm, this approach requires a refined reparameterization of the data and its associated residuals to ensure numerical stability. Such an adaptation could be implemented within established open-source frameworks such as BERT (Günther *et al*., 2006) or ResIPy (Rücker *et al*., 2017). The proposed framework is therefore best viewed as complementary to existing systems.

Practical feasibility

In this framework, the survey lines need not be strictly linear; they may follow curved or irregular paths as long as electrode coordinates are accurately defined in 3D. This flexibility allows layout adaptation to terrain or target geometry and naturally fits the concept of multidirectional current flow.

Although the method requires greater field effort and additional equipment—particularly recording systems capable of handling a larger number of channels—it can still be implemented feasibly under realistic survey conditions. Many of these difficulties are expected to be mitigated through technical creativity and gradual instrument development. The most natural implementation of the proposed horizontal-vector framework is through autonomous, self-contained measurement nodes, conceptually similar to the autonomous receiver nodes now widely used in seismic acquisition**.** Each node would integrate two orthogonal electrode pairs for horizontal vector measurement and a data logger with GPS-based timing synchronization, operating without cable connections to a central control unit. Such nodes could be distributed freely across a survey area — in regular grids, irregular patches, or any configuration dictated by terrain and logistical constraints — while current injection can be performed in the conventional manner using multi-core cables along accessible lines. Because the electrode pairs within each node need not share a common global orientation, they may also be rotated as required to accommodate local deployment

conditions while preserving horizontal-vector measurement capability. For subsequent inversion and interpretation, the orientation of each rotated electrode pair must therefore be recorded as part of the survey geometry. This decoupling of the current source from the potential measurement units is a key operational advantage of the proposed approach.

A particularly significant application arises in areas where equipment or personnel access is severely limited, such as steep terrain, buildings, water bodies, or restricted zones. As illustrated in Figure 10, the current-electrode path need not coincide with the node locations and may pass through, around, or entirely outside the node-distribution area, depending on access and survey design. The survey geometry thereby adapts to physical constraints while minimizing reductions in spatial coverage — a capability that is fundamentally unavailable to conventional cable-dependent ERT systems.

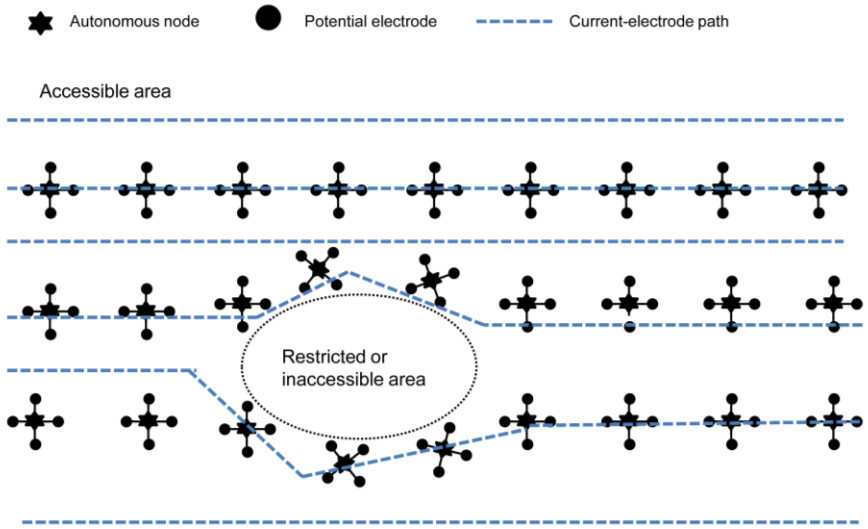

Figure 10. Conceptual illustration of flexible 3D ERT acquisition enabled by horizontal-vector measurements. The current-electrode path follows accessible routes, while autonomous measurement nodes are distributed independently across the survey area, including within restricted or inaccessible regions. This decoupling allows survey geometries beyond conventional line-based configurations.

This acquisition concept also opens the possibility of multidirectional current injection, in which data from multiple source orientations are combined within a single survey framework. The FAViP-based geometric factor introduced in this study provides the consistent normalization required for such data, so that apparent resistivity values remain physically meaningful across arbitrary source–receiver geometries. In this respect, the concept is analogous to modern node-based acquisition in 3D seismic surveys, where autonomous receiver nodes enable flexible and high-density recording

geometries without cable connections. Whether multidirectional acquisition leads to substantially improved subsurface sensitivity in ERT remains an open question. Because DC electric fields diffuse broadly through the subsurface, the incremental benefit of multidirectional current injection may be more limited than wide-azimuth effects in seismic surveys. Nevertheless, the proposed framework provides the normalization basis required to investigate this question systematically, and the autonomous node concept offers the acquisition flexibility needed to test it in practice.

It should also be noted that pole–pole arrays already allow relatively flexible electrode deployment and remain one of the most basic acquisition schemes in 3D ERT. However, their spatial resolution is limited, and they do not directly provide horizontal-vector measurements. The present framework is therefore directed not merely toward geometric flexibility, but toward the physically consistent acquisition and normalization of horizontal electric-field information.

CONCLUSIONS

This study presented an approach to horizontal-vector measurement in 3D ERT together with a corresponding geometric factor for non-collinear horizontal measurements. The framework employs the primary-field orientation, calculated for a homogeneous medium based on the specific current-electrode configuration of the survey site, as a consistent geometric reference, enabling direction-consistent normalization of potential differences for arbitrary electrode geometries. This approach formalizes a unified geometric basis that remains valid for curved survey paths and non-collinear layouts. Analytical tests in a homogeneous half-space confirmed that the generalized geometric factor recovers the true resistivity with negligible error under practical conditions. Although not a full 3D validation, an illustrative 2D inversion comparison further suggested that the total horizontal potential difference can provide more representative and less distorted apparent-resistivity inputs than conventional inline-only data, particularly where the surface electric field deviates significantly from the survey-line direction.

The proposed approach may broaden the azimuthal coverage of ERT acquisition beyond conventional straight survey lines by allowing more flexible current-electrode layouts and potential-measurement configurations. By providing a physically consistent framework, the proposed concept may offer a basis for improved directional characterization of 3D ERT responses in complex environments.

This work provides a theoretical foundation and conceptual framework. The central contribution lies in formalizing the physical principle that potential-difference standardization should be aligned

with the local primary-field direction — a principle long implicit in conventional collinear configurations but never explicitly generalized for arbitrary electrode geometries. Full 3D inversion validation and field-scale implementation remain important subjects for future research.

ACKNOWLEDGEMENTS

The author gratefully acknowledges Subsurface Information Technologies, Inc. for providing the necessary resources and environment to conduct this research. The author also wishes to thank Prof. Sándor Szalai for his valuable guidance on this paper and for his insightful comments and helpful discussions regarding this work. Special thanks are also extended to Prof. In-Ky Cho of Kangwon National University for his constructive suggestion on the necessity of formulating geometric factors for non-collinear arrays, which greatly motivated this study.

CONFLICT OF INTEREST STATEMENT

The author declares that aspects of the methodology described in this work are related to a patent application filed by Subsurface Information Technologies, Inc., with which the author is affiliated. No commercial funding or financial compensation was received in connection with this study.

REFERENCES

Bibby, H. M. (1977) The apparent resistivity tensor. *Geophysics* 42, 1258–1261. https://doi.org/10.1190/1.1440791

Bibby, H. M., Risk, G. F. (1973) Interpretation of dipole-dipole resistivity surveys using a hemispheroidal model. *Geophysics* 38, 719-736. https://doi.org/10.1190/1.1440371

Bièvre, G., Oxarango, L., Günther, T., Goutaland, D., Massardi, M. (2018) Improvement of 2D ERT measurements conducted along a small earth-filled dyke using 3D topographic data and 3D computation of geometric factors. *Journal of Applied Geophysics* 150, 80–90. https://doi.org/10.1016/j.jappgeo.2018.04.012

Günther, T., Rücker, C., Spitzer, K. (2006) Three-dimensional modeling and inversion of DC resistivity data incorporating topography — Part I: Modelling. *Geophysics* 71, G153–G161. https://doi.org/10.1190/1.2338332

Jung, H.-K., Min, D.-J., Lee, H.-S., Oh, S., Chung, H. (2009) Negative apparent resistivity in dipole-dipole electrical surveys. *Exploration Geophysics* 40, 33–40. https://doi.org/10.1071/EG08111

Keller, G. V., Furgerson, R., Lee, C. Y., Harthil, N., Jacobson, J. J. (1975) The dipole mapping method. *Geophysics* 40, 451-472. https://doi.org/10.1190/1.1440539

Loke, M.H., Barker, R. D. (1996) Practical techniques for 3D resistivity surveys and data inversion. *Geophysical Prospecting* 44, 499–523. https://doi.org/10.1111/j.1365-2478.1996.tb00162.x

Parasnis, D. S. (1975) *Mining Geophysics*. Elsevier.

Risk, G. F., Macdonald, W. J. P., Dawson, C. B. (1970) D.C. resistivity surveys of the Broadlands geothermal region, New Zealand. *Geothermics* 2, 287–295. https://doi.org/10.1016/0375-6505(70)90027-1.

Rücker, C., Günther, T., Wagner, F. M. (2017) pyGIMLi: An open-source library for modelling and inversion in geophysics. *Computers & Geosciences* 109, 106–123. https://doi.org/10.1016/j.cageo.2017.07.011

Szalai, S., Szarka, L., Prácser, E., Bosch, F., Müller, I., Turberg, P. (2002) Geoelectric mapping of near-surface karstic fractures by using null arrays. *Geophysics* 67, 1769–1778. https://doi.org/10.1190/1.1527077

Szalai, S., Szarka, L. (2008a) On the classification of surface geoelectric arrays. *Geophysical Prospecting* 56, 159–175. https://doi.org/10.1111/j.1365-2478.2007.00673.x

Szalai, S., Szarka, L. (2008b) Parameter sensitivity maps of surface geoelectric arrays I. Linear arrays, *Acta Geodetica et Geophysica Hungarica*. 43, 419–437. https://doi.org/10.1556/AGeod.43.2008.4.4

Szalai, S., Szarka, L. (2008c) Parameter sensitivity maps of surface geoelectric arrays II. Nonlinear and focussed arrays, *Acta Geodetica et Geophysica Hungarica*. 43, 439–447. https://doi.org/10.1556/AGeod.43.2008.4.5

Tejero-Andrade, A., Cifuentes, G., Chávez, R. E., López-González, A. E., Delgado-Solórzano, C. (2015) L- and CORNER-arrays for 3D electric resistivity tomography: an alternative for geophysical surveys in urban zones. *Near Surface Geophysics* 13, 553–563. https://doi.org/10.3997/1873-0604.2015015

Varga, M., Novák, A., Szarka, L. (2018) Application of tensorial electrical resistivity mapping to archaeological prospection. *Near Surface Geophysics* 6, 39-48. https://doi.org/10.3997/1873-0604.2007030

Yi, M.-J., Kim, J.-H., Chung, H.-S. (2003) Enhancing the resolving power of least-squares inversion with active constraint balancing. *Geophysics* 68, 31-41. https://doi.org/10.1190/1.1581045